




Cite this: *Phys. Chem. Chem. Phys.*,  
2023, 25, 25492

# A theoretical study based on coherent perfect absorption and polarization separation in one-dimensional magnetized plasma photonic crystals

Fu Pei Wu, Jia Tao Zhang and Hai Feng Zhang \*

This article presents a study on tunable narrowband coherent perfect absorption (CPA), which can be altered by adjusting the initial phase to the ranges of  $1.03\alpha$ – $1.13\alpha$  (with  $\alpha = 2\pi c/d$ ) and  $1.29\alpha$ – $1.43\alpha$ . The relative bandwidths of these ranges are determined to be 8.5% and 7.4%, respectively. The study utilizes the transfer matrix method for calculations of the largest CPA amplitudes within one-dimensional (1D) magnetized plasma photonic crystals (MPPCs) across two absorption bands, achieving a maximum of 0.99 and 0.98, respectively. In addition, the phase modulation and amplitude modulation characteristics of the CPA are also discussed, and the results show that its absorption amplitude can be gradually modulated from 0.08 to 0.99 by the former and from 0.60 to 0.98 by the latter. The external magnetic fields have also been shown to limit the CPA amplitude between 0.41 and 0.99 within one band and between 0.52 and 0.99 within another band. The study further highlights the effect of plasma frequency and dielectric layer thickness on coherent band shifts towards high or low frequencies. Notably, the article presents the multiband polarization separation properties of 1D MPPCs, with calculated transmittance differences between the TM and TE waves of up to 0.70 and 0.74 at  $1.13\alpha$  and  $1.37\alpha$ , respectively.

Received 15th May 2023,  
Accepted 15th August 2023

DOI: 10.1039/d3cp02216a

rsc.li/pccp

## 1. Introduction

Research regarding photonic crystals (PCs) has increased due to their ability to exhibit photonic band gaps<sup>1–3</sup> that are similar to those observed in semiconductor materials.<sup>4,5</sup> This property has inspired researchers to explore the integration of various advanced materials, including plasma,<sup>6–8</sup> into PCs. Periodic arrangements of dielectric components may guide the propagation of electromagnetic waves with frequencies below the plasma frequency within the plasma.<sup>6</sup> The use of external magnetic fields for modifying the optical characteristics of metamaterials has been widely employed in various research pursuits, such as optical Tamm states<sup>9</sup> and nonlinear optics.<sup>10</sup> In this study, we introduce the concept of tunable narrow-band coherent perfect absorption (CPA), which is an optical property that can be achieved by incorporating a lossy plasma medium within the layered structure of PCs. The impact of the magneto-optical Voigt effect on the absorption characteristics of TM waves by plasma is investigated herein. Notably, a significant alteration in the absorption of TM waves is observed when a

magnetic field is applied perpendicular to the propagation direction of the electromagnetic (EM) wave.<sup>11</sup>

This study focuses on the interference of forward and backward transmitted EM waves in magnetized plasma photonic crystals (MPPCs) to attain CPA.<sup>12–14</sup> Previous research conducted by Longhi in 2011 investigated the time-reversed laser procedure in a two-energy medium with uniform widening in the optical cavity, which further established the necessary conditions for CPA.<sup>15</sup> The current findings suggest that CPA may have significant implications for numerous optical switching phenomena and present a valuable contribution to the field. Relevant literature on this topic is referenced.<sup>16–18</sup> In 2018, Huang and colleagues demonstrated the achievement of polarization-independent multiband CPA through the use of a hypersurface.<sup>19</sup> However, once the structure is determined for multiband absorption, as the frequency becomes fixed, it requires a fresh sample to be produced in order to cater to different frequencies of EM waves by altering the radius, thereby creating challenges for industrial manufacturing processes. In 2019, Wang *et al.* studied CPA laser points (CPA-LPs) in anti-parity-time symmetric photonic crystals. By varying the gain–loss factor and angular frequency, they identified single-frequency points of CPA corresponding to reflectance and transmittance poles.<sup>20</sup> In 2021, an investigation on CPA at a

College of and Optical Engineering & College of Flexible Electronics  
(Future Technology), Nanjing University of Posts and Telecommunications, Nanjing,  
210023, China. E-mail: hanlor@163.com

single frequency point in the GHz band with a layer-by-layer periodic structure has been conducted by Wu *et al.* Coherent absorption with a tunable range of 0.12–0.99 has been experimentally achieved at the specific frequency point of interest.<sup>22</sup> The challenge in achieving narrow-band CPA is characterized by meeting the requisite that the phase difference between the reflection and transmission coefficients should assume certain predetermined values within the frequency domain. The present study provides a valuable contribution towards understanding these dilemmas.

In the present study, a comprehensive calculation of the reflection ( $r$ ) and transmission ( $t$ ) coefficients of MPPCs is carried out by employing the transfer matrix method (TMM). Additionally, the condition for CPA is presented using the TMM. Notably, we delve into the potential of tunable CPA in terms of phase and amplitude modulation, exploring the impact of parameters such as the magnetic field, plasma frequency in the magnetized plasma layer and the thickness of the medium. Furthermore, the modifications made to the structure of MPPCs revealed the emergence of distinct polarization separation properties within a corresponding frequency band, enabling the selective transmission of either TE or TM waves.

## 2. Design and discussion

### 2.1. Theoretical model

MPPCs are arranged along the  $z$ -direction according to “ABABDFABCAB-BACBAFDBABA”, where the thickness of  $D$  is  $d_4 = 0.04d$  and the thickness of  $F$  is  $d_5 = 0.06d$ , which denote two separate magnetized plasma layers, respectively.  $d = 2\pi c/\omega_{p0}$  is the normalization constant,<sup>11</sup> where the definition of the plasma frequency ( $\omega_{p0}$ ) is given in the subsequent discussion, and  $c$  is the speed of light in a vacuum.  $d_1 = 0.015d$ ,  $d_2 = 0.06d$ , and  $d_3 = 0.08d$  are the thicknesses of media A, B, and C, respectively, and their dielectric constants are  $\epsilon_A = 10$ ,  $\epsilon_B = 3.4$ , and  $\epsilon_C = 5.9$ , respectively. Media 1–3 are all artificially composed hyperbolic metamaterials that consist of multiple materials in order to achieve the desired refractive index for composite design. Under the TM or TE mode, the forward and backward EM waves incident at an angle of incidence of  $\theta$  are

denoted by  $I^+$  and  $I^-$ , respectively, and  $O^+$  and  $O^-$  represent the output EM waves after passing through the given MPPCs (Fig. 1).<sup>11</sup>

### 2.2. Calculation method

The dielectric function of an anisotropic plasma layer under the action of an applied magnetic field has the following form:<sup>11</sup>

$$\epsilon = \begin{pmatrix} \epsilon_1 & 0 & i\epsilon_2 \\ 0 & \epsilon_3 & 0 \\ -i\epsilon_2 & 0 & \epsilon_1 \end{pmatrix} \quad (1)$$

where<sup>11</sup>

$$\begin{aligned} \epsilon_1 &= 1 - \frac{\omega_p^2(\omega + i\nu)}{\omega[(\omega + i\nu)^2 - \omega_c^2]}, \\ \epsilon_2 &= 1 - \frac{-\omega_p^2\omega_c}{\omega[(\omega + i\nu)^2 - \omega_c^2]}, \\ \epsilon_3 &= 1 - \frac{\omega_p^2}{\omega(\omega + i\nu)} \end{aligned}$$

The incident wave frequency, plasma frequency, collision frequency and cyclotron frequency are denoted by  $\omega$ ,  $\omega_p$ ,  $\nu$  and  $\omega_c$ , respectively. This study employs the classical Drude model to describe the influence of the plasma ionization degree, where  $\omega_p = q^2 n_e / (\epsilon_0 m_0)$ ,<sup>24</sup>  $n_e = 10^{18} \text{ m}^{-3}$  is the plasma density,  $q = 1.6 \times 10^{-19} \text{ C}$  and  $m_0 = 9.1 \times 10^{-31} \text{ kg}$  are the charge and mass of the electron, respectively,  $\epsilon_0 = 8.8542 \times 10^{-12} \text{ F m}^{-1}$  is the dielectric constant under vacuum,  $\nu = 0.09\omega_p$ ,  $\omega_{c1} = qB_1/m_0 = 0.48\omega_p$  is the cyclotron frequency of plasma layer  $D$  at a magnetic field of  $B_1$  and  $\omega_{c2} = qB_2/m_0 = 0.95\omega_p$  is the cyclotron frequency of plasma layer  $F$ . The effective dielectric functions of the plasma layer in TM and TE modes are<sup>11</sup>

$$\epsilon_{\text{TM}} = \frac{\epsilon_1^2 - \epsilon_2^2}{\epsilon_1}, \quad \epsilon_{\text{TE}} = 1 - \frac{\omega_p^2}{\omega(\omega + i\nu)} \quad (2)$$

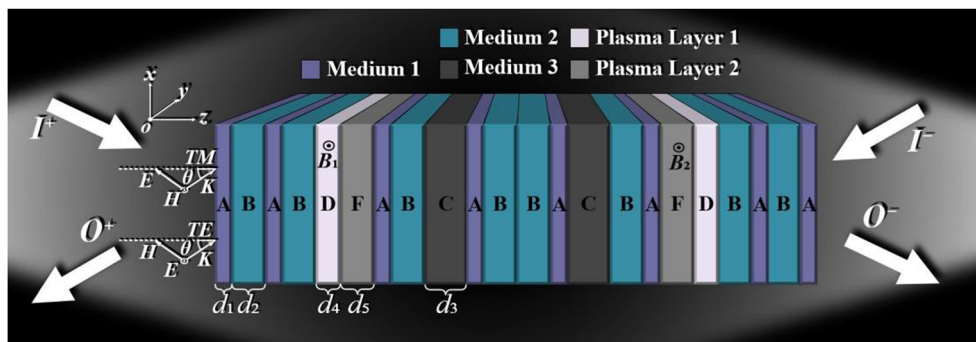


Fig. 1 Schematic diagram depicting bi-directional oblique incident ( $I^+$ ,  $I^-$ ) and transmitted ( $O^+$ ,  $O^-$ ) electromagnetic waves in 1D MPPCs under different polarization modes.

Under the TE mode, the transfer matrix has the following form:<sup>11</sup>

$$M_{TE} = \begin{pmatrix} \cos \delta & -\frac{i}{\eta} \sin \delta \\ -i\eta \sin \delta & \cos \delta \end{pmatrix} \quad (3)$$

where  $\delta = (2\pi/\lambda)d_x n \cos \theta$ , ( $x = 1..6$ ),  $\eta = (\epsilon_0/\mu_0)^{1/2} n/\cos \theta$ ,  $\theta = \arcsin(n_0 \sin \theta_0/n)$ , where  $n = \epsilon^{1/2}$ ,  $\theta$  are the refractive index and incident angle of the layer, respectively.  $n_0 = 1$  and  $\theta_0 = 0^\circ$  are the refractive index and the incident angle of air,  $\mu_0 = 4\pi \times 10^{-7} \text{ N m}^{-1}$  is the vacuum permeability. On the other hand, the transfer method has the following form under the TM mode:<sup>11</sup>

$$M_{TM} = \begin{pmatrix} \cos \delta + \frac{k^z \epsilon_2}{k^x \epsilon_1} \sin \delta & -\frac{i}{\eta} \left[ 1 + \left( \frac{k^z \epsilon_2}{k^x \epsilon_1} \right)^2 \right] \sin \delta \\ -i\eta \sin \delta & \cos \delta - \frac{k^z \epsilon_2}{k^x \epsilon_1} \sin \delta \end{pmatrix} \quad (4)$$

where  $\eta = (\epsilon_0 \epsilon_{TM}/\mu_0)^{1/2}/\cos \theta$ ,  $k^x = k_{TM} \cos \theta$ ,  $k^z = k_{TM} \sin \theta$ , and  $k_{TM} = (\epsilon_{TM} \omega^2/c^2)^{1/2}$ . For the dielectric layer A, B or C, its corresponding transfer matrix corresponds to eqn (3) regardless of any mode.

The action of MPPCs on incident waves is calculated using the TMM:<sup>11</sup>

$$M = M_A M_B M_A M_B M_D \cdots M_D M_B M_A M_B M_A = \begin{vmatrix} M_{11} & M_{12} \\ M_{21} & M_{22} \end{vmatrix} \quad (5)$$

$r$  and  $t$  have the following forms:<sup>11</sup>

$$r = \frac{(M_{11} + M_{12}\eta_0)\eta_0 - (M_{21} + M_{22}\eta_0)}{(M_{11} + M_{12}\eta_0)\eta_0 + (M_{21} + M_{22}\eta_0)} \quad (6)$$

$$t = \frac{2\eta_0}{(M_{11} + M_{12}\eta_0)\eta_0 + (M_{21} + M_{22}\eta_0)}$$

where  $\eta_0 = (\epsilon_0/\mu_0)^{1/2}/\cos \theta$ , and the intrinsic absorptance ( $A_b$ ) is<sup>11</sup>

$$A_b = 1 - |r|^2 - |t|^2 \quad (7)$$

We generalize the relationship between the incident ( $I^+$ ,  $I^-$ ) and output ( $O^+$ ,  $O^-$ ) EM waves at both ends through the scattering matrix  $S$  as<sup>21</sup>

$$\begin{bmatrix} O^+ \\ O^- \end{bmatrix} = S \begin{bmatrix} I^+ \\ I^- \end{bmatrix} = \begin{bmatrix} t^- & r^+ \\ r^- & t^+ \end{bmatrix} \begin{bmatrix} I^+ \\ I^- \end{bmatrix} \quad (8)$$

CPA ( $A_C$ ) in the sensor is expressed as<sup>21</sup>

$$A_C = 1 - \frac{|O^+|^2 + |O^-|^2}{|I^+|^2 + |I^-|^2}$$

$$= 1 - (|t| - |r|)^2 - 2|tr| \left( 1 + \cos \varphi_1 \cos \varphi_2 \frac{2|I^+||I^-|}{|I^+|^2 + |I^-|^2} \right) \quad (9)$$

where  $\varphi_1$  and  $\varphi_2$  are the phase differences between  $r$  and  $t$ , and the incident waves, respectively. From eqn (9), it can be derived that  $A_C$  can be achieved when  $t = \pm r$ ,  $\cos \varphi_1 \cos \varphi_2 = -1$  and  $|I^-| = |I^+|$ .

### 2.3. Analysis and discussion

By assuming equal amplitudes of incident waves propagated in the forward and backward directions and  $\varphi_2$  being either 0 or  $\pi$ , the present study reveals that the  $A_C$  is induced whenever  $t = r$  and  $\cos \varphi_1 \cos \varphi_2 = -1$  holds true throughout the MPPCs. These findings are well demonstrated in Fig. 2(a) and (b), whereby for frequencies in the range of  $1.03\alpha$ – $1.13\alpha$  or  $1.29\alpha$ – $1.43\alpha$  ( $\alpha = 2\pi c/d$ ), the values of  $t$  and  $r$  are found to be approximately 0.5, whilst the value of  $\cos \varphi_1$  is near  $-1$  or  $1$  within the respective bands. In accordance with the TM mode, Fig. 2(c) demonstrates that the  $A_C$  amplitude exceeds 0.90 for the coherence condition within the frequency band. The relative bandwidths for frequency bands  $1.05\alpha$ – $1.14\alpha$  and  $1.30\alpha$ – $1.40\alpha$  lie at 8.5% and 7.4%, respectively, with the highest value of  $A_C$  registered at 0.99 for  $1.07\alpha$ . It can be clearly seen that as the initial phase changes from 0 to  $\pi$ , the absorption amplitude within the low-frequency coherent band (blue) decreases, while the absorption amplitude within the high-frequency band (pink) increases. Therefore, phase modulation not only allows for frequency control but also enables control over the absorption amplitude. On the other hand, the magnetized plasma layer under the TE mode exhibits similar traits as to when it is non-magnetized. As a result, Fig. 2(d) illustrates that the coherence condition is not met and the absorption amplitude remains low. These new findings demonstrate an innovative way of polarization separation through the utilization of the CPA principle.

This paper investigates the transmission of two opposite EM waves, which are delineated as a signal wave and a control wave. The interaction between these standing waves and the MPPCs is determined by their location in the waves, where there is a weak interaction at the wave node and a high interaction at the wave belly, leading to enhanced coherent absorption. Consequently, controlling the phase and intensity of the control wave leads to changes in the intensity of the output signal wave. To optimize the absorption effect, the  $A_b$  of a single beam of EM waves traversing the MPPCs should be 0.50. In this case, by adjusting the phase of the control wave, 100% optical modulation will be achieved. On the other hand, 50% modulation can be achieved by modulating the relative amplitude of the control and signal waves.

Tunable absorption amplitude is difficult to achieve for most devices, and the majority of research is based on adjusting the existing structure or adding more lossy media. The modulation of absorption amplitude by external fields has attracted extensive attention from researchers in the field of coherent absorption.<sup>22</sup> The findings presented in Fig. 3(a) show that the amplitude of narrow-band  $A_C$  within the frequency range of  $1.29\alpha$  to  $1.43\alpha$  gradually decreases to 0.55 as the value of  $\cos \varphi_2$  shifts from  $-1$  to 0. The amplitude corresponds to  $A_b$  in the range that attains  $A_C$ . The amplitude of the absorption band within the frequency range of  $1.03\alpha$  to  $1.13\alpha$  is gradually increased to 0.98 as  $\cos \varphi_2$  increases from 0 to 1. These observations indicate that the proposed tunable CPA band not only is capable of modulating the absorption amplitude by  $\cos \varphi_2$  but also enables the transfer of narrow-band

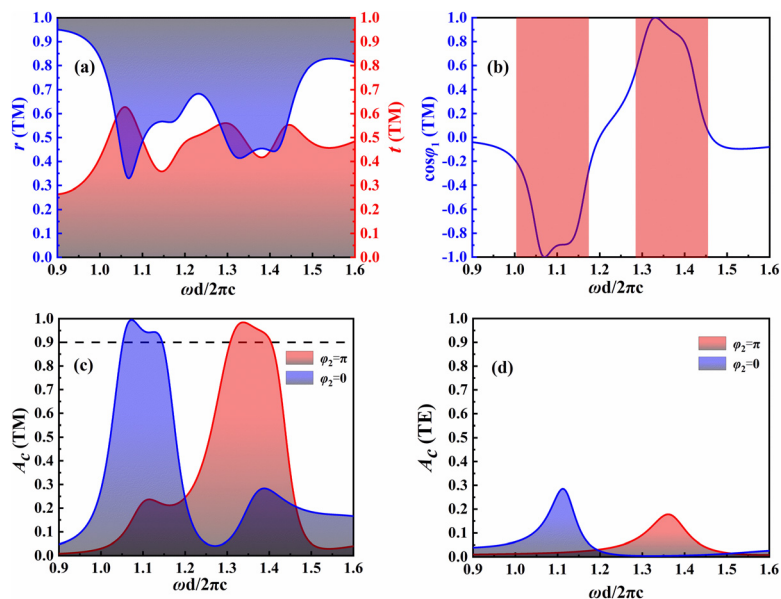


Fig. 2 Under the TM mode, (a) the relationship between the amplitude of  $t$  of a forward transmitted EM wave and  $r$  of a backward propagating wave in a coherent band. (b) The phase difference between  $t$  and  $r$ ; the pink identification band corresponds to the frequency band where the narrow-band CPA is located. (c)  $A_c$  when the initial phase difference between the incident waves on both sides is 0 or  $\pi$ . (d) The corresponding  $A_c$  in the coherence band when the polarization mode is TE wave.

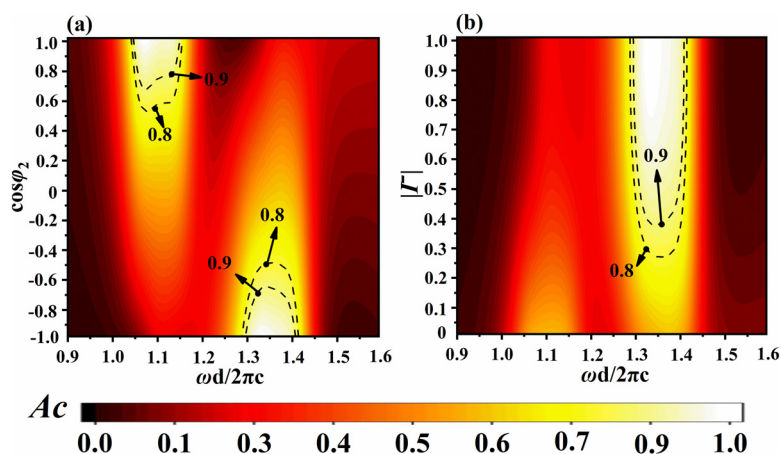


Fig. 3 (a) and (b) Two-dimensional (2D) plane view of narrow-band  $A_c$  modulated by  $\varphi_2$  or  $|\Gamma|$ .

absorption within the GHz band. This provides valuable insights for the design of multi-frequency absorbers and filters. The fundamental principle of phase modulation lies in the capability to manipulate the position of MPPCs within the standing wave field that emerges during signal and control wave transmission. This can be achieved by altering the phase difference, ultimately leading to the modulation of the  $A_c$ . Fig. 3(b) illustrates the control exerted on the  $A_c$  by the modulation of the relative intensity of the two incident waves at  $\cos\varphi_2 = -1$ . The results indicate that the amplitude modulation is only 50% efficient. Furthermore, the absorption amplitude in the  $1.29\alpha$ – $1.43\alpha$  band increases with the variation in relative intensity from 0 to 1, which corresponds to the absorption at  $|\Gamma| = 0$  for the  $A_b$ . These observations are

consistent with previous findings in a metamaterial discussed by Zhang *et al.*<sup>23</sup>

The present study sheds light on the effects of plasma as a loss medium and the role of  $A_c$  in MPPCs. As per the coherence condition satisfaction in two coherent bands, the transmittance ( $T$ ) and reflectance ( $R$ ) of the unidirectional transmitted EM wave in the TM mode are expected to be equal. The modulation efficiency peaks when the value reaches 0.25, leading to the complete absorption of the bidirectional incident TM wave. Conversely, applied magnetic fields do not modulate the EM wave transmitted with TE polarization, and  $T$  remains unaltered within the coherent band. As a result, the MPPCs proposed in this study present polarization separation capabilities.

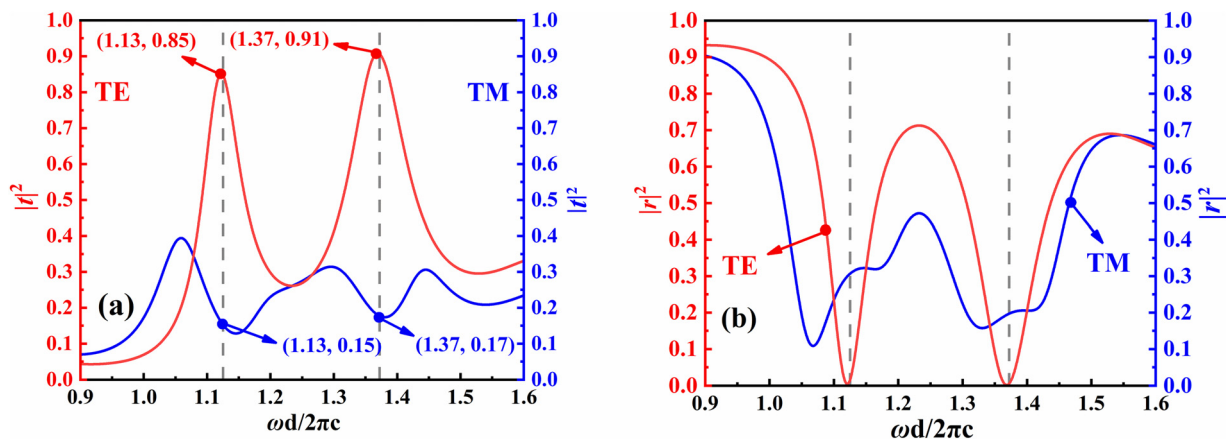


Fig. 4 The polarization separation phenomenon within the coherence band under different incident polarization modes: (a) transmission and (b) reflection of electromagnetic waves.

The  $T$  value for the TE mode of the incident wave passing through the structure in the coherent band ranging from  $1.03\alpha$  to  $1.15\alpha$  is calculated to be at a maximum of 0.85 at  $1.13\alpha$  (as shown in Fig. 4(a)), while the  $T$  for the TM mode at this frequency point is estimated to be 0.15. The study finds that

vertical and horizontal polarization can also be selected in another absorption band. At a frequency of  $1.37\alpha$ ,  $T$  is calculated to be 0.91 for TE mode incidence, while for TM mode incidence, it is 0.17 at that point. At  $1.25\alpha$ , the  $T$  values for different modes of incident waves are equal. In addition, the

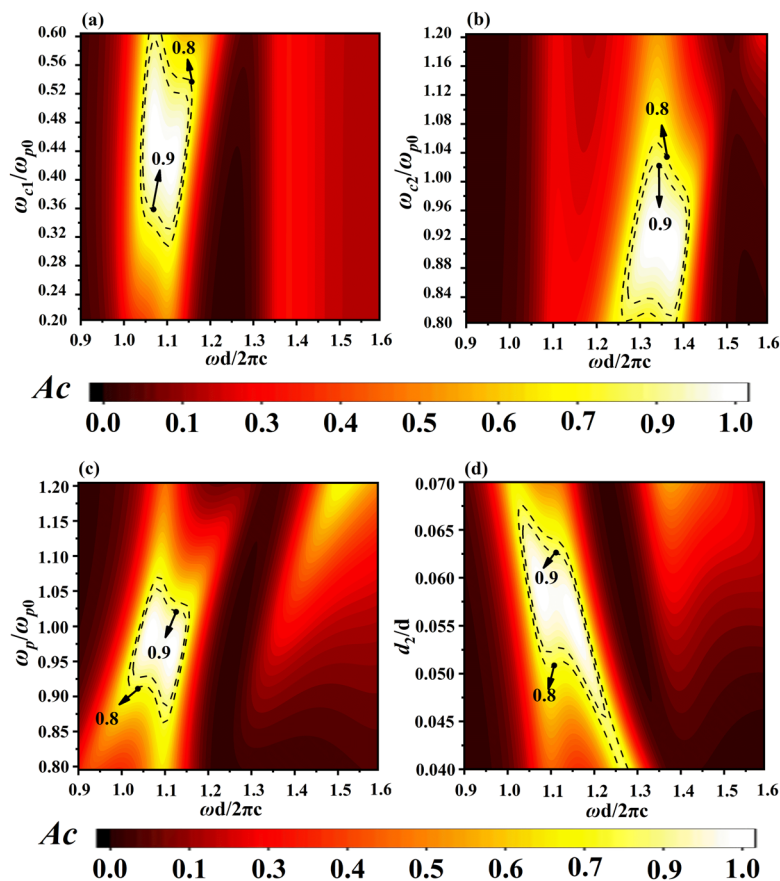


Fig. 5 (a) When  $\varphi_2 = 0$ , the 2D plane view of  $A_C$  is influenced by the magnetic field  $B_1$  which is applied to plasma layer D. (b) When  $\varphi_2 = \pi$ ,  $A_C$  is influenced by the magnetic field  $B_2$  which is applied to plasma layer F. (c) and (d) When  $\varphi_2 = 0$ , the coherent band is controlled by  $\omega_p$  and  $d_2$  to move in the direction of the high frequency or low frequency region.

resonance points at 1.05 and 1.45 are caused by the variation of the effective permittivity of different plasma layers. Both plasma layers D and F have an imaginary part of the effective permittivity greater than zero, indicating that the two observed resonance peaks originate from the absorption of different magnetized plasmas. The reflected energy of an incident electromagnetic wave in different modes within the coherent band is shown in Fig. 4(b). The interference of electromagnetic waves in TM modes incident within the coherent band leads to perfect absorption, wherein the reflection and transmission wave amplitudes must remain similar in order to achieve perfect dissipation. In contrast, the reflected energy of TE mode incident electromagnetic waves is negligible, and a vast majority of the polarization state incident energy can effectively penetrate the photonic crystal, resulting in the separation of the incident electromagnetic waves under different polarization modes.

The study reveals that, in the presence of  $\varphi_2$ , the  $A_C$  emerges in separate frequency bands, and the amplitudes are contingent on the magnetic field embedded in the separate plasma layers, as can be observed from Fig. 4. Notably, the coherence band is between  $1.03\alpha$  and  $1.15\alpha$  when  $\varphi_2 = \pi$ , as depicted in Fig. 5(a). It is observed that narrow-band absorption first increases and then decreases as  $\omega_{c1}$  rises. Additionally, when  $\omega_{c1}$  is in the range of  $0.36\omega_{p0}$ – $0.52\omega_{p0}$ , the absorption amplitude is greater than 0.90. Since the probability of matching the

$\omega_c$  is outside this range with the EM wave frequency and  $\nu$  is quite small, it results in the absorption being insignificant. Based on the findings presented in Fig. 5(b), when  $\varphi_2 = 0$ , the coherent band moves between  $1.27\alpha$  and  $1.42\alpha$ . It is also observed that the absorption amplitude is greater than 0.90 in the frequency range of  $0.84\omega_{p0}$ – $0.98\omega_{p0}$ , but it decreases considerably outside this frequency range. The absorption of EM waves by plasma is because the electrons in the plasma are excited by the electric field of the incident EM waves and absorb the energy of the EM waves, while transferring the energy to neutral particles and ions through collisions. Furthermore, it is noted that in the TM mode the excited electrons are accelerated by the applied magnetic field, consequently leading to increased absorption.

The results depicted in Fig. 5(c) and (d) demonstrate the capability of shifting the absorption band by varying either the value of  $\omega_p$  or the thickness of the dielectric layer. Observations show that when  $\varphi_2 = 0$  an increase in  $\omega_p$  leads to a movement of the absorption band towards the higher frequency side. In the case where  $\omega_p$  is fixed at  $\omega_{p0}$ , a relative bandwidth above 0.90 is observed to attain a maximum value of 8.55%. This wide absorption band occupies the frequency range of  $1.03\alpha$  to  $1.15\alpha$ , which is presented in detail in Fig. 5(c). Increasing the thickness of dielectric B has been observed to shift the coherent band towards the lower frequency region. Correspondingly, the absorption amplitude is observed to increase and subsequently

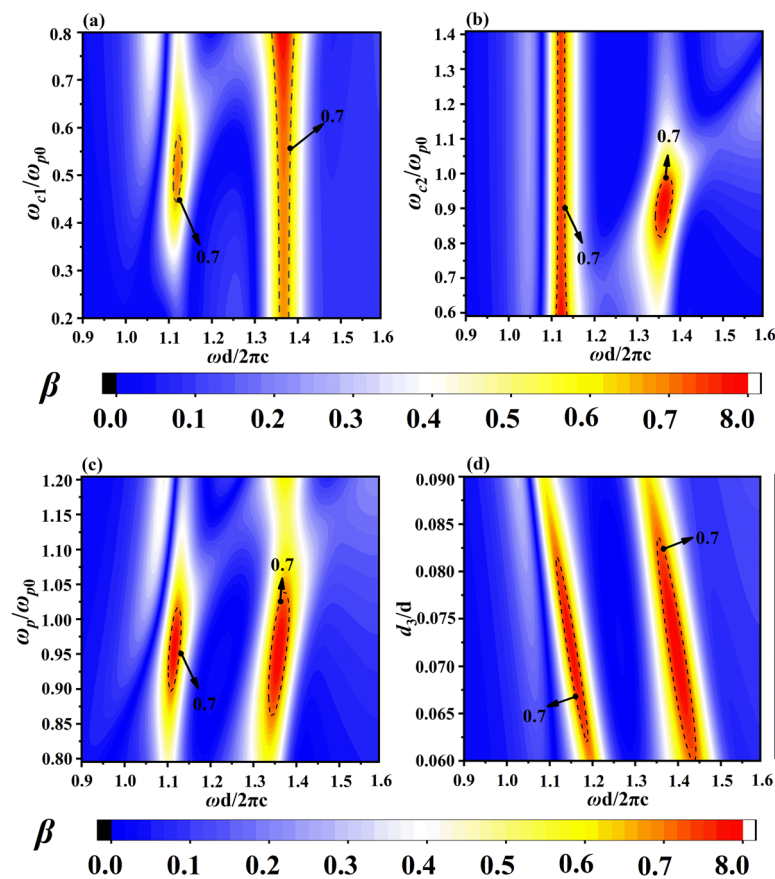


Fig. 6 (a) and (b) The separation bands located at the lower or higher frequency bands are modulated by the applied magnetic field strength on the different plasma layers. (c) and (d) The separation band is controlled by  $\omega_p$  and  $d_3$  to move in the direction of the high frequency or low frequency region.

undergo rapid diminution with an increasing value of  $d_2$ . The relative bandwidth is reported to attain a maximum value of 8.55% when the thickness of dielectric B, denoted as  $d_2$ , is  $0.06d$ . Further, the maximum absorption efficiency reaches up to 0.99 in this situation. Notably, the findings when  $\varphi_2 = \pi$  align with the earlier discussion and have been therefore excluded from the present argument.

This study investigates the interaction between the applied magnetic field and the polarization separation performance, as observed in Fig. 6(a) and (b). Specifically, it is demonstrated that the magnetic field due to different layers has a distinct influence on the polarization separation performance across varying frequency ranges. To quantify the degree of polarization separation, we employ the parameter  $\beta$ , defined as  $\beta = |T_{TE} - T_{TM}|$ . Notably, the value of  $\beta$  with a maximum value of 0.70 is observed to be influenced by layer D that is subjected to an applied magnetic field strength of  $B_1$ , when the separation band is located in the range of  $1.03\alpha$ – $1.15\alpha$ . It is further noted that changes in the value of  $B_1$  do not seem to affect the value of  $\beta$  observed at higher frequencies. In contrast, layer F subjected to an applied magnetic field strength of  $B_2$  seems to affect the separation band located at higher frequencies, namely,  $1.29\alpha$ – $1.43\alpha$ , where  $\beta$  attains a maximum value of 0.74.

This paper explores the impact of adjusting both  $\omega_p$  and  $d_3$  on the frequency shift of defective modes in the structure, as well as on the position and width of the separation band. Critically, the position of the separation band can be controlled by adjusting both  $\omega_p$  and  $d_3$ , resulting in its movement towards either high- or low-frequency regions. Additionally, the width of the band is also modulated simultaneously. Fig. 6(c) highlights the impact of  $\omega_p$  on the separation band. The figure depicts a clear shift of the separation band towards high frequencies with an increase in  $\omega_p$ , accompanied by a rise-and-fall pattern in its degree of separation. It is worth noting that the region marked by the line corresponds to  $\beta$  values greater than 0.70, and the separation bands near  $1.10\alpha$  and  $1.35\alpha$  display the highest values of  $\beta$ , which are 0.74 and 0.75, respectively. In addition, Fig. 6(d) reveals the influence of  $d_3$  on the separation band. The thickness of dielectric C brings about a change in the position of the band gap inside the PCs. As shown in Fig. 6(d), an increase in the dielectric thickness results in the shift of the separation band towards lower frequencies. The maximum values of  $\beta$  within the separation band near  $1.15\alpha$  and  $1.40\alpha$  are found to be as high as 0.74 and 0.75, respectively.

### 3. Conclusion

The parameters of the proposed structure were determined using the TMM, revealing tunable narrow-band  $A_C$  located in the ranges of  $1.03\alpha$ – $1.15\alpha$  and  $1.27\alpha$ – $1.42\alpha$ . The  $A_C$  was found to display a remarkable phase modulation up to 89% and amplitude modulation up to 43%. Notably, bidirectional tuning of the  $A_C$  amplitude and position can be attained by adjusting the applied magnetic field and material parameters. Furthermore, the study explores the  $\beta$  between various polarization modes,

reporting maximum values of 0.70 and 0.74 at  $1.13\alpha$  and  $1.37\alpha$ , respectively. It is worth noting that optimizing the structural parameters allows for fine-tuning of the separation position and control of  $\beta$  values. Overall, the findings of this study hold the potential for numerous applications, such as multi-band absorbers, optical switches, and antenna design.

### Conflicts of interest

There are no conflicts to declare.

### Notes and references

- 1 E. Yablonovitch, *Phys. Rev. Lett.*, 1987, **58**, 2059–2062.
- 2 S. John, *Phys. Rev. Lett.*, 1987, **58**, 2486.
- 3 H. L. Ma, B. M. Liang, S. L. Zhuang, J. B. Chen, Q. Jiang and J. W. Ding, *Opt. Lett.*, 2016, **41**, 3833–3835.
- 4 A. H. Aly, D. Mohamed and M. A. Mohaseb, *Int. J. Mod. Phys. B*, 2019, **33**, 1950397.
- 5 A. H. Aly and F. A. Sayed, *Int. J. Mod. Phys. B*, 2020, **34**, 30462.
- 6 H. Hojo, K. Akimoto and A. Mase, *Otsu*, 2003, 347.
- 7 L. M. Qi, *J. Plasma Phys.*, 2016, **82**, 905820111.
- 8 Y. Zheng, Z. Yi, L. Liu, X. W. Wu, H. Liu, G. F. Li, L. C. Zeng, H. L. Li and P. H. Wu, *Appl. Thermal Eng.*, 2023, **230**, 120841.
- 9 J. T. Zhang, S. S. Rao and H. F. Zhang, *Phys. B*, 2022, 639.
- 10 Z. W. Gong, W. Xu, N. A. Liedienov, D. S. Butenko, I. V. Zatovsky, I. A. Gural'skiy, Z. Y. Wei, Q. J. Li, B. B. Liu, Y. A. Batman, A. V. Pashchenko and G. G. Levchenko, *Phys. Chem. Chem. Phys.*, 2022, **24**, 21872.
- 11 L. M. Qi, Z. Q. Yang, F. Lan, X. Gao and Z. J. Shi, *Phys. Plasmas*, 2010, **17**, 042501.
- 12 Y. D. Chong, G. Li, C. Hui and A. D. Stone, *Phys. Rev. Lett.*, 2010, **105**, 53901.
- 13 W. J. Wan, Y. D. Chong, L. Ge, H. Noh, A. D. Stone and H. Cao, *J. Sci.*, 2011, **331**, 889–892.
- 14 Y. D. Chong and A. D. Stone, *Phys. Rev. Lett.*, 2011, **107**, 163901.
- 15 S. Longhi, *Phys. Rev. A*, 2011, **83**, 055804.
- 16 J. H. Shi, X. Fang, T. F. Rogers, E. Plum, K. F. Macdonald and N. I. Zheludev, *Opt. Exp.*, 2014, **22**, 21051–21060.
- 17 S. A. Mousavi, E. Plum, J. H. Shi and N. I. Zheludev, *Appl. Phys. Lett.*, 2014, **105**, 011906.
- 18 X. Fang, K. F. Macdonald and N. I. Zheludev, *Light Sci-Appl.*, 2015, **4**, 292.
- 19 S. Huang, Z. W. Xie, W. D. Chen, J. Q. Lei and F. L. Wang, *Opt. Exp.*, 2018, **26**, 7066.
- 20 H. L. Wang, W. H. Kong, P. Zhang, Z. M. Li and D. Zhong, *Appl. Sci.*, 2019, **9**, 2738.
- 21 W. Zhu, F. Xiao, K. Ming and M. Premaratne, *Appl. Phys. Lett.*, 2016, **108**, 121901.
- 22 F. P. Wu, H. Zhang, B. F. Wan and H. F. Zhang, *Phys. Scri.*, 2021, **96**, 125868.
- 23 J. F. Zhang, K. F. MacDonald and N. I. Zheludev, *Light Sci-Appl.*, 2012, **1**, 18.
- 24 V. L. Ginzberg, *The propagation of electromagnetic waves in plasmas*, Pergamon, New York, 1970.